NASA Technical Memorandum 101413
AIAA-89-0609

Evaluation of Three Turbulence Models for the Prediction of Steady and Unsteady Airloads

Jiunn-Chi Wu
Georgia Institute of Technology
Atlanta, Georgia

Dennis L. Huff
Lewis Research Center
Cleveland, Ohio

and

L.N. Sankar
Georgia Institute of Technology
Atlanta, Georgia

Prepared for the
27th Aerospace Sciences Meeting
sponsored by the American Institute of Aeronautics and Astronautics
Reno, Nevada, January 9-12, 1989

NASA

EVALUATION OF THREE TURBULENCE MODELS FOR THE PREDICTION OF STEADY AND UNSTEADY AIRLOADS

Jiunn-Chi Wu*
Georgia Institue of Technology, Atlanta, GA 30332

Dennis L. Huff**
NASA Lewis Research Center, Cleveland, OH 44135

L. N. Sankar***
Georgia Institute of Technology, Atlanta, GA 30332

ABSTRACT

Two-dimensional and quasi-3D Navier-Stokes solvers have been used to predict the static and dynamic airload characteristics of airfoils. The following three turbulence models were used: (1) Baldwin-Lomax algebraic model, (2)Johnson-King ODE model for maximum turbulent shear stress and (3) A two equation k-e model with law-of-the-wall boundary conditions. It was found that in attached flow the three models gave good agreement with experimental data. In unsteady separated flows, these models gave only a fair correlation with experimental data.

INTRODUCTION

The flow field surrounding modern rotorcraft and propeller configurations is highly complex, and is dominated by three-dimensional effects, transonic flow, flow separation and unsteadiness, and can be properly modeled only through the numerical solution of the 3-D unsteady Navier-Stokes equations. Since full 3-D simulations are costly, historically researchers have used simpler 3-D analyses such as the lifting line theory, which use a table look up of 2-D steady and unsteady airfoil characteristics. The airfoil tables needed may come from carefully performed experiments, or from 2-D computer codes. To be useful, the 2-D computer codes should provide:

1. Reliable prediction of airfoil static load data and dynamic stall characteristics.

2. A method for evaluation of the flow yaw effects on airload characteristics.

3. A suitable turbulence model for properly modeling separated flows.

In this study, 2-D and quasi-3D computer codes have been developed capable of predicting the static and dynamic load characteristics of straight and swept wings. Three turbulence models are currently operational. These are: (1) Baldwin-Lomax algebraic model, (2) Johnson-King ODE model and (3) Two-equation k-ϵ model. This paper describes the performance of the above two computer codes for a variety of steady and unsteady flow conditions. The effects of turbulence model on the predicted flow properties are also evaluated.

* Graduate Research Assistant, Student Member AIAA. Presently, Associate Professor, National Central University, Taiwan.

** Research Engineer, Member AIAA

*** Associate Professor, Member AIAA.

MATHEMATICAL AND NUMERICAL FORMULATION

In this work, the unsteady 2-D and quasi-3D, Reynolds averaged, compressible Navier-Stokes equations are solved in a body-fitted coordinate system using an alternating direction implicit (ADI) procedure. The mathematical formulation has been described in detail in References 1 and 2, and only a brief outline of the formulation is given here.

Governing Equations

The equations governing unsteady three-dimensional flow are the full Navier-Stokes equations, and may be written in a Cartesian coordinate system as:

$$q_t + F_x + G_y + H_z = R_x + S_y + T_z \quad (1)$$

Here, q is the unknown flow properties vector; F, G and H are the inviscid flux vectors; R, S and T are the viscous terms. The purpose of the present work is to compute the unsteady viscous flow over arbitrary configurations undergoing arbitrary motion. To facilitate this, the following general curvilinear coordinate system is used:

$$\xi = \xi(x,y,z,t)$$

$$\eta = \eta(x,y,z,t)$$

$$\zeta = \zeta(x,y,z,t)$$

$$\tau = t \quad (2)$$

In such a coordinate system, equation (1) may be written in the following strong conservation form:

$$q_\tau + F_\xi + G_\eta + H_\zeta = R_\xi + S_\eta + T_\zeta \quad (3)$$

The quantities q , F , G , H , R , S , T are related to their Cartesian counterparts through the metrics of transformation.

In such a general coordinate system, the airfoil surface maps onto a ζ = Constant surface. The radial direction is associated with the η coordinate, and the direction normal to the airfoil maps onto ξ = constant lines or planes. For a detailed description of the flow and flux vectors in the cartesian and transformed coordinate systems, the reader is referred to Ref. 1.

Infinite Sweep Assumption

In many applications involving flow over rotor blades, and propellers, the flow in regions away from the root and the tip may be assumed to be invariant along the spanwise direction. That is, a large spanwise or radial component of flow may exist, but the derivatives of

the flow properties along the radial or spanwise direction may be assumed negligible. This assumption is sometimes called the "infinite sweep" assumption and is often used in the aircraft industry to compute three-dimensional boundary layers, and to investigate their stability characteristics. Under the assumptions of infinite sweep, the above equations become

$$q_\tau + F_\xi + H_\zeta = R_\xi + T_\zeta \quad (4)$$

The equation set (4) consists of 5 equations, corresponding to the conservation of mass, energy, and u,v,w momentum along the x,y and z directions respectively. In the special case where the blade sweep angle is zero, and the yaw angle of the flow relative to the blade is zero, the spanwise or radial component of velocity v is identically zero, and the momentum equation along the y- direction may be neglected, resulting in 4 equations.

Solution Procedure

The above equations are parabolic in time, and may be advanced in time using a suitable stable, dissipative scheme. In the present work, a formulation similar to that described by Steger [Ref. 2] was used. Standard second order accurate central differences were used to approximate the spatial derivatives, and to compute the metrics of transformation. The highly non-linear flux terms F and H, which are unknown at a given time level 'n' were linearized about their values at a previous time level 'n'. The time derivative was approximated as a first order accurate, two-point, backward difference. This leads to a system of simultaneous equations for the flow vector q^{n+1}. These equations were re-expressed as a penta-diagonal matrix system of simultaneous equations for the 'delta' quantity $(q^{n+1} - q^n)$. The penta-diagonal equation system was approximately factored into a product of tridiagonal matrices using the Beam-Warming approximate factorization scheme, as discussed in Ref. 1.

Artificial Viscosity Model

The use of standard differences to approximate the spatial derivatives can give rise to growth of high frequency errors in the numerical solution with time. To control this growth, a set of artificial dissipation terms were added to the discretized equations. These dissipation terms used a combination of second and fourth order differences of the flow properties, in a manner discussed by Jameson et al. [Ref. 3].

TURBULENCE MODELS

As stated earlier, three turbulence models were considered in this work. These models are briefly descried here.

Baldwin-Lomax Model

This model is patterned after the well known Cebeci-Smith model, and has been extensively used by a number of researchers [Ref. 2,4]. It uses a two layer formulation to model the eddy viscosity. In the inner layer, the following expression is used.

$$\mu_t \quad \alpha \quad l^2 \, |(uy - vx)| \qquad (5)$$

where l is the "mixing length" measured as the distance of the point from the nearest solid surface, modified by the classical van Driest damping term, and the von Karman's constant . In the outer layer, the eddy viscosity is written as

$$\mu_t \quad \alpha \quad F_{max} \, Y_{max} \qquad (6)$$

where F_{max} and Y_{max} represent the turbulent velocity and length scales in the outer part of the boundary layer. The quantity F_{max} is computed as the maximum of the following function:

$$F(y) = y \, |(u_y - v_x)| \, [1 - \exp(-y\rho_w \tau_w / 26\mu_w)] \quad (7)$$

where y is the distance of the point from the nearest solid wall. Y_{max} is the y- location where F(y) reaches a maximum. The quantities ρ , τ and μ are the density, shear stress and viscosity respectively. The subscript 'w' represents conditions at the wall.

The Klebanoff intermittency factor is used to drive the eddy viscosity to zero far away from the boundary layer. In the wake regions downstream of the blade trailing edge, Baldwin-Lomax model is used with minor modifications. For a detailed discussion of this model, the reader is referred to Ref. 4.

Johnson-King One Equation Model

The Baldwin-Lomax model is an equilibrium model in the sense that is assumes that the eddy viscosity instantaneously adjusts to the local flow characteristics. The Baldwin-Lomax model thus does not take into account the upstream eddy viscosity or turbulent kinetic energy values. Johnson-King model attempts to rectify this situation, by solving an ordinary differential equation (ODE) for the maximum turbulent kinetic energy within the boundary layer at a given streamwise location. This ODE may be thought of as a simplified form of the Reynolds stress equation .This ODE is solved as an initial value problem by marching along the flow direction, and automatically brings into the account the upstream history of the flow.

The eddy viscosity μ_t is assumed to be

$$\mu_t = \mu_{to} \, [1 - \exp(\mu_{tl}/\mu_{to})] \quad (8)$$

where

$$\mu_{tl} = 0.4 \, \rho \, D^2 \, y \, k_m \qquad (9)$$

and

$$\mu_{to} = 0.0168 \, \rho \, \sigma(x) \, u_e \, \delta^* \, \gamma \quad (10)$$

Here D is the van Driest damping function, y is the distance from the wall, and k_m is the maximum Reynolds shear stress at the current x- location. Furthermore, γ is the Klebanoff intermittency factor, ue is the edge velocity, δ^* is the displacement thickness, and $\sigma(x)$ is a modeling parameter.

An ordinary differential equation is used to model the streamwise development of turbulent kinetic energy, and is given by

$$k_m^{1/2} = (k_m^{1/2})_{eq} - [L_m \, u_m / (a_1 k_m)] \, dk_m/dx \; - D_m \, L_m / k_m \quad (11)$$

The quantities D_m , L_m , a_1 are empirically prescribed as done in Reference 5. The subscript m over some of the quantities indicates that these quantities are computed at the y- location where the local shear stress is maximum. The quantity $(k_m)_{eq}$ is computed from equations 8 , 9 and 10 with the value of $\sigma(x)$ assumed unity. The quantity $\sigma(x)$ is iteratively determined, so that the value of the eddy viscosity computed from equations 8 , 9 and 10 and the maximum shear stress computed using equation (11) satisfy the following relationship:

$$k_m = \mu_{tm} / \rho \; |(u_y + v_x)|_m \qquad (12)$$

For an efficient iterative procedure for computing $\sigma(x)$, and the empirical relationships used in the Johnson-King model, the reader is referred to Ref. 5.

Gorski's k-ϵ Model

The third turbulence model considered in this work is the well known k-ϵ model, implemented with a set of wall boundary conditions proposed by Gorski [Ref. 6]. This model requires numerical solution of

two partial differential equations for the instantaneous values of turbulent kinetic energy k, and the dissipation rate ϵ at every point in the flow field. These equations may be formally written as

$$(\rho k)_t + (\rho uk)_x + (\rho vk)_y = (\mu_k k_x)_x + (\mu_k k_y)_y + S_1$$

$$(\rho e)_t + (\rho ue)_x + (\rho ve)_y = (\mu_e \epsilon_x)_x + (\mu_e \epsilon_y)_y + S_2 \qquad (13)$$

Here μ_k and μ_e are eddy viscosities controlling the diffusion of k and ϵ; S_1 and S_2 are source terms which describe the production and dissipation rates of k and ϵ. As in the case of the original flow equations, these equations and their three-dimensional counterparts may be cast in a strong conservation form in a moving, body-fitted, curvilinear coordinate system. In the present work these equations were solved as a 2 x 2 system of partial differential equations using an ADI procedure similar to that used to solve the mean flow equations, after the mean flow has been updated at a given time level.

In the vicinity of the solid wall, the values of k and ϵ computed from the above equations were overwritten with values computed from the following assumed relationships for k and ϵ:

$$k = C y^2$$

$$\epsilon = \text{Constant}$$

These constants were evaluated using the values of k and ϵ computed at nodes well within the logarithmic region of the boundary layer, in a manner documented in detail by Gorski [6].

RESULTS AND DISCUSSIONS

Steady Flow Studies Using the Baldwin-Lomax Model

A series of steady viscous calculations were performed using the Baldwin-Lomax model. In Figs. 1-5, a number of flow results are shown in the form of surface pressures, loads, skin friction and velocity profiles for a NACA 0012 airfoil and a supercritical RAE 2822 airfoil at a variety of flow conditions and compared with experimental data. The following flow conditions are considered:

Case 1 :Surface pressure distribution over NACA 0012 airfoil at free stream Mach number M_∞ = 0.301, Angle of Attack α = 13.5 degrees, Reynolds number based on chord, Re = 3.9 million.

Case 2: Static load characteristics for a NACA 0012 airfoil at M_∞ = 0.301, Re = 3.9 million.

Case 3: Predicted lift curve slope $dC_l/d\alpha$ versus freestream Mach number for a NACA0012 airfoil at α = 0 deg., Re = 9.0 million.

Case 4: Surface pressure distribution over a RAE 2822 airfoil at corrected M_∞ = 0.73, corrected α = 2.79 deg., Re = 6.5 Million.

Case 5: Skin friction coefficient and velocity profiles on the upper airfoil surface for a RAE 2822 airfoil at M_∞ = 0.73, α = 2.79 deg., Re = 6.5 million.

As seen in Fig. 1, good agreement was found between the computed surface pressures and experiment [7] at a high angle of attack flow prior to static stall. The static load characteristics of the NACA 0012 airfoil shown in Fig. 2 indicate good prediction of static lift and moment stall. However, the drag was overpredicted at high angles of attack. In these calculations, the transition effects on loads prediction were simulated by enforcing the transition point at 0.05% chord on both the upper and lower surfaces. In Fig. 3, a good agreement for the lift curve slope is observed between the present predictions and the experiment [8]. For the super-critical RAE 2822 airfoil it is found that the predicted surface pressures shown on figure 4 are in good agreement with the experiment [9] over most of the airfoil. The predicted pressure expansion near the leading edge on the upper airfoil surface is not as strong as observed in the experiment, presumably because the flow was assumed to be turbulent over the entire airfoil surface in the present calculations. The integrated lift and drag from the experiment are 0.7433 and 0.0127, respectively, which compare well with the values of 0.7432 and 0.0134 from the present code. Fig. 5 shows that the skin friction in predicted well except near the trailing edge. The computed velocity profiles at two chordwise locations are in good agreement with the experiment.

Additional viscous flow calculations computed using this solver may be found in Ref. 1.

Dynamic Stall of Oscillating Airfoils Computed Using Baldwin-Lomax Model

A number of dynamic stall calculations have been performed for several 2-D airfoils and a swept wing configuration with infinitely long span. The airfoils analyzed in the 2-D mode are a NACA 0012 airfoil and two modern helicopter airfoil sections (the Sikorsky SC-1095 airfoil and the Hughes HH-02 Airfoil). The 2-D dynamic stall results are presented in Figs. 6 Through 13. The angle of attack variation during the dynamic stall is given by α = 15 - 10 cos(ωt). The free stream Mach number in these three cases was 0.28, the Reynolds number based on chord was 3.7 Million, and the reduced frequency based on semi-chord was 0.15.

The calculations were carried out for two cycles of airfoil pitching motion starting with a steady state solution at 5 degree angle of attack, to remove influence of flow transients. Here results for the second cycle are shown. In figure 6, the dynamic stall calculations are presented for two grids: a 157 x 58 grid and a 253 x 58 grid.

As can be seen in Fig. 6, predicted loads using the coarse grid agree with experiments [7] reasonably well during the upstroke. Although the maximum lift coefficient is underpredicted and moment prediction was less accurate, the theory still clearly captures the moment and lift stall. The leading edge separation occurred when the angle of attack is 17 degree during the upstroke. A large "primary" vortex formed subsequently. As the airfoil incidence increased, this primary vortex passed along the airfoil surface and was shed into the wake at an angle of attack around 25 degrees. During the downstroke, however, the agreement between the numerical results and experimental data is not good. A secondary vortex from the trailing edge was shed during the downstroke. It appears that the strength of the secondary vortex is overpredicted (which takes place at a between 25 to 23 degrees). As the incidence of the airfoil continues to decrease, the agreement between predicted and measured loads improves.

The dynamic stall predictions for the Hughes HH-02 airfoil and the Sikorsky SC-1095 airfoil are shown in Figs. 7 and 8. Good agreement between the theory and experiment is also observed during the upstroke for these two cases. During the downstroke, the computed results are only in fair agreement with the experimental data. Overall level of agreement for these two airfoils is similar to that for the NACA 0012 airfoil.

In order to evaluate the effects of yaw angle on static and dynamic load characteristics, a series of calculations which take into account the effect of the blade sweep relative to the freestream, and thus the effect of radial flow on the load characteristics, have been done. In Fig. 9, the static lift versus angle of attack are shown for a NACA 0012 airfoil at 0.3 Mach number and Re=2.7 million at 30 degree yaw angle. Comparisons with the experimental data of Carta [10] are also given. Good agreement between the two sets of data is observed.

In Figs. 10 and 11, the dynamic stall load characteristics of a NACA 0012 airfoil at 0 and 30 yaw angle are compared. The flow conditions are: M_∞ =0.3, Re=2.7 million. For comparison, Carta's results are also given. Only a qualitative agreement between the two sets of data is observed. The yaw effects on dynamic stall hysteresis loops are predicted to be less profound than observed in experiment. Several factors may contribute to the discrepancies. Firstly, the

location of transition is somewhat different between the two sets of data. In the computation, the flow is assumed to be fully turbulent over the entire airfoil. In Carta's experiments transition depended on factors such as surface roughness, mean flow turbulence level, etc. and is difficult to model. Secondly, three-dimensional effects of the swept wing with finite span considered in the experiment may be important and the present quasi three-dimensional approximation may not suitable for this configuration.

TURBULENCE MODEL STUDIES

In order to assess the effects of turbulence models on the prediction of separated flows, a number of turbulent flow solutions have been computed using the three turbulence models and have been compared with each other and also with available experimental data. Several steady flow situations were considered. These are: turbulent boundary layer over a flat plate; attached subsonic flow over airfoil; and separated transonic flow over an airfoil. Following these studies, calculations were made for an airfoil experiencing dynamic stall, using higher order turbulence models.

Attached Flows

First, some results are presented for a turbulent boundary layer developing over a flat plate at zero angle of attack. The flow is nearly incompressible and the Reynolds number is five million [11]. The calculations were performed on a computational region which extended half plate length upstream and downstream of the flat plate, and one plate length above the plate surface; 151 equally spacing nodes were used along the streamwise and 51 nodes were placed at geometrically increasing distance in the normal direction. The first point off the surface located within a y+ of 2. The predicted surface skin friction and velocity profile at mid-plate are shown in Fig. 12 for the three models. These three models predict results that compare very well with experiment. Note that velocity characteristics of the sublayer and buffer regions were correctly captured by these models. This resolution is crucial to the success of turbulence model in resolving the near-wall turbulent flow characteristics.

Next results are presented for a turbulent attached flow past an airfoil. Fig. 13 shows computed and experimental pressure distributions for the NACA 0012 airfoil at an attached flow condition (M_∞ = 0.301 , α = 13.5 degrees and Re = 3.9 million). The computed surface pressures are in good agreement with experimental data [7]. It should be mentioned that the Johnson-King model which requires solution of an ODE starting from a user-prescribed point has some uncertainty as to where it should be activated. The activating location should be a finite distance downstream of stagnation point or transition location. Several locations were tested (x/c ranging from 0.08 to 0.25) and it was found the solution in this case was not affected by the starting location.

Transonic Flows with Separation

Two transonic flow cases exhibiting mild and strong separation have been computed and compared with detailed turbulent flow measurements. In Fig. 14, the surface pressures are shown for a NACA 0012 airfoil at experimental conditions [8]:M_∞ = 0.899, Angle of attack = 2.66 deg., Re = 9 Million. It is seen that the Baldwin-Lomax and the k-ϵ models predict similar pressure distributions, with a shock predicted stronger than the measurements. The predicted pressure distribution using the Johnson-King model is dependent on where the non-equilibrium formulation is activated. The location x/c = 0.15 gives best agreement with measured surface pressures. However, it is not clear how a starting location may be chosen.

The NACA 64A010 airfoil at a shock induced stall condition [12] (M_∞ = 0.8, α = 6.2 deg., Re = 2 Million) has also been considered for detailed turbulent flow comparisons. As can be seen in Fig. 15, the predicted pressure distributions are not in good agreement with experiment for any of the models. All of them predicted too strong and aft a shock and too little pressure recovery. It was found that the Johnson-King model (the activation location of the non-equilibrium calculation was chosen at x/c = 0.15) predicted a shock location forward of the other models. It should be mentioned that all these models showed some unsteadiness (5%) in their loads predictions (buffeting). Mean velocity and Reynolds shear stress profiles for this case are compared in Fig. 16. Except in the close-to the-wall and near-wake regions, reasonable agreement with the measured mean-velocity profiles is found for all the three models. Because of the thick boundary layer predicted and the underprediction of pressure recovery, the predicted mean velocity profiles do not match well with experimental data close to the wall and this effect also extends to the near-wake region(x/c = 1.02). Poor predictions are found for Reynolds shear stress profiles for all of the models. The shear stress peaks are underpredicted and their locations shift more closer to the wall compared to experimental data.

The behavior of the k-ϵ model is somewhat similar to the Baldwin-Lomax algebraic model in this case. However, a thinner reversed flow is observed using the k-ϵ model. Additionally, the k-ϵ model shows a better prediction of the Reynolds shear stress profiles close to the wall.

From the two transonic flow cases just described, it appears that the k-ϵ model does not hold any noticeable advantage over the simple Baldwin-Lomax model in predicting the shock-induced separated flows. It has been pointed out by Lakshminarayana [13] that the k-ϵ model does not predict the separation point or the reattachment any more accurately. Therefore, inaccurate predictions of velocity and Reynolds shear stress profiles in the separated regions were not surprising.

As for the Johnson-King model, it is seen that the solutions depend on the choice of activation location of the non-equilibrium calculation at least in separated flows. This shows that the optimum location differs from flow to flow. For unsteady, separated flow such as the dynamic stall problem, it would be difficult to determine the optimum location during the oscillating airfoil motion. In addition, calculations using the Johnson-King model tend to show small oscillations about mean loads for the steady cases and require more iterations than other two models to ensure convergence. Thus, it is concluded that the Johnson-King model is not suitable for predicting the unsteady, highly separated flows. In dynamic stall calculations to be discussed next, only the Baldwin-Lomax algebraic model and k-ϵ equation model were used and compared.

Unsteady, Highly Separated Flow (Dynamic Stall Case)

The dynamic stall calculation for NACA 0012 airfoil previously reported was repeated for an comparison of the k-ϵ and the Baldwin-Lomax models for this complex flow. Predicted aerodynamic loads are presented in Fig. 17 and compared with experiment [7]. The k-ϵ model predicts higher lift during the upstroke. During the downstroke, predictions using the k-ϵ model show trends similar to the Baldwin-Lomax model, except that a smaller second vortex shedding (around 24 deg.) and much stronger third vortex-shedding (around 15 deg.) were detected. Results from both models only show a qualitative agreement with the experiment during the downstroke.

COMPUTER TIME REQUIREMENTS

The calculations presented in this work were performed on a CRAY X/MP supercomputer at the NASA Lewis Research Center. The computer time for a viscous solution using the Baldwin-Lomax model is 0.28 second per time step using a 157 x 58 grid. A converged viscous steady solution requires 2000 to 3000 time steps when a space-varying time step technique is employed (roughly equal to 850 seconds). For dynamic stall cases, the computer time required for a full cycle on a 157x58 and a 253x58 grid was 4100 seconds and 6600 seconds, respectively. The swept wing configuration, requires 20% more computing time than the 2-D version, because an additional (spanwise momentum) equation needs to be solved. Computer time for the Johnson-King model is about 0.30 seconds per time step, and requires about 500 to 1000 more time steps than the Baldwin-Lomax model to achieve a steady state. For the k-ϵ model, one time step requires 0.34 seconds and the same number of time steps as the algebraic Baldwin-Lomax model are needed to achieve a steady solution.

CONCLUSIONS

An efficient solution procedure has been used to provide improved prediction of complex flow phenomena associated with rotor flows. The two-dimensional, and quasi-three dimensional, compressible, full Navier-Stokes equations have been solved using an ADI scheme. Numerical results show that good prediction of static loads and dynamic stall hysteresis loops of rotor blade sections was feasible. Evaluation of three eddy viscosity models have been made. In attached flows the three turbulence models considered gave good correlation with experimental data. For strongly separated flows, eddy viscosity models available including the k-ϵ model are not adequate. No clear trend could be found favoring the use of higher order turbulence models in separated flows.

ACKNOWLEDGEMENTS

The turbulence modeling work was supported by the NASA Lewis Research Center under Grant No. NAG 3-768. Studies related to the effect of yaw angle were supported by a grant from the McDonnell Douglas Helicopter Company. The authors wish to thank Dr. L.S. King of the NASA Ames Research Center for providing the Johnson-King turbulence model subroutine.

REFERENCES

1. Wu, Jiunn-Chi., "A Study of Unsteady Turbulent Flow past Airfoils," Ph. D. Thesis, Georgia Institute of Technology, June 1988.

2. Steger, J. L.," Implicit Finite Difference Simulation of Flow about Arbitrary Two-Dimensional Geometries, " AIAA Journal, Vol. 18, No. 7 July, 1978, pp. 679-686.

3. Jameson, A., Schmidt, W. and Turkel, E., "Numerical Solutions of the Euler Equations by Finite Volume Methods Using Runge-Kutta Time Stepping Schemes," AIAA Paper 81-1259.

4. Baldwin, B.S. and Lomax H., "Thin Layer Approximation and Algebraic Model for Separated Turbulent Flows," AIAA Paper 78-0257.

5. Johnson, D.A. and King, L.S., "A Mathematically Simple Turbulence Closure Model for Attached and Separated Turbulent Boundary Layers," AIAA Journal, Vol. 23, No. 11, Nov. 1985, pp. 1684-1692.

6. Gorski, J.J. "A New Near-Wall Formulation for the k-e Equations of Turbulence," AIAA Paper 86-0556.

7. McAlister, K.W., Pucci, S.L., McCroskey, W. L. and Carr, L.W., "An Experimental Study of Dynamic Stall in Advanced Airfoil Sections, Vol 2, Pressure and Force Data," NASA TM 84245, Sept, 1982.

8. Harris, C.D., "Two-Dimensional Aerodynamic Characteristics of the NACA 0012 Airfoil in the Langley 8-foot Transonic Pressure Tunnel," NASA TM-81927, 1981.

9. Cook, P.H. McDonald, M.A. and Firmin, M.C.P., "Aerofoil RAE 2822 Pressure Distributions, and Boundary Layer and Wake Measurements,"AGARD Advisory Report No. 138, May 1979.

10. St. Hilaire, A.O. and Carta, F.O., "Analysis of Unswept and Swept Wing Chordwise Pressure Data From an Oscillating NACA 0012 Airfoil Experiment," NASA CR 3567, Vol I-Technical Report, March 1983.

11. Weighardt, K. and Tillmann, W., "On the Turbulent Friction Layer for Rising Pressure," NACA TM 1314, 1951.

12. Johnson, D.A. and Bachalo, W.D., "Transonic Flow past a Symmetrical Airfoil-Inviscid and Turbulent Flow Properties," AIAA Journal, Vol. 18, Jan. 1980, pp. 16-24.

13. Lakshminarayana, B., "Turbulence Modeling for Complex Flows," AIAA Paper 85-1653, 1985.

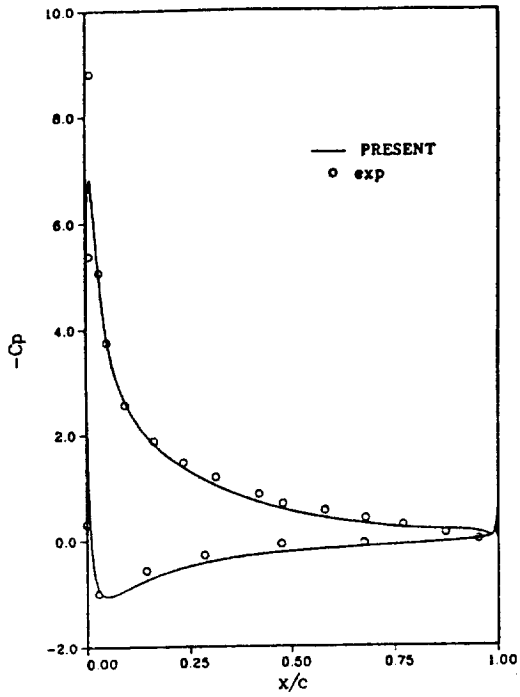

1. Surface Pressure Distribution over a NACA 0012 Airfoil at M_∞ = 0.301, α = 13.5 degrees, Reynolds Number = 3.9 Million.

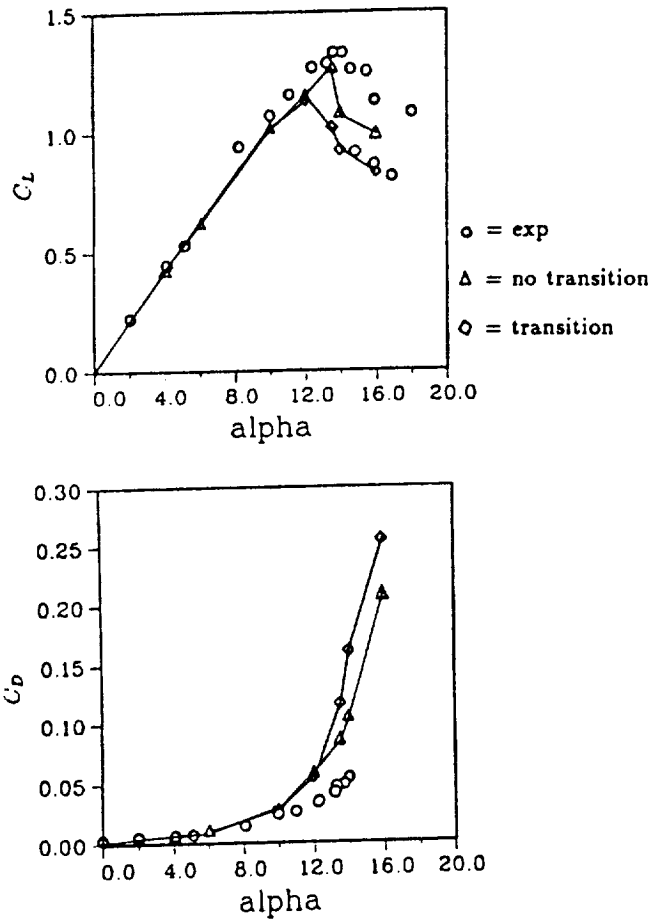

2 Computed and Measured Static Loads over a NACA 0012 Airfoil at M_∞ = 0.3 , Re = 3.9 Million.

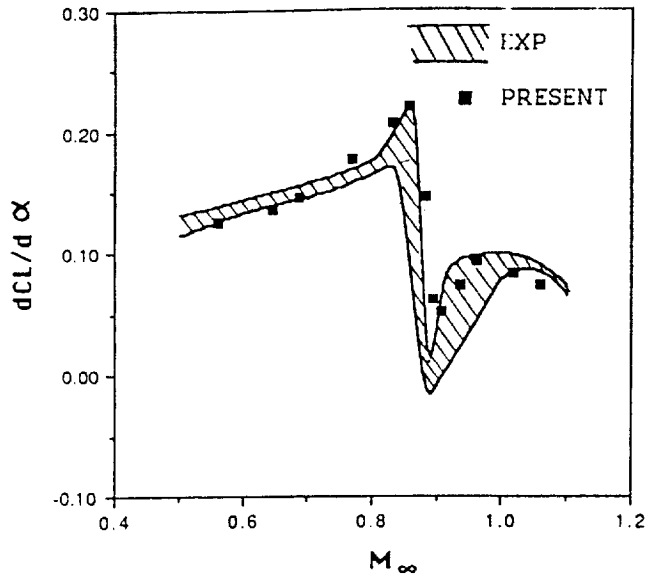

3. Predicted and Measured Lift Curve Slope vs. Mach Number for a NACA 0012 Airfoil at α = 0 degrees, Re = 9 Million.

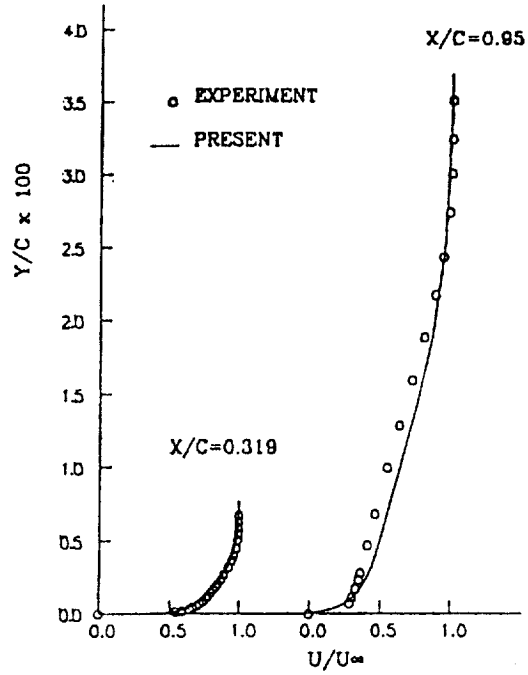

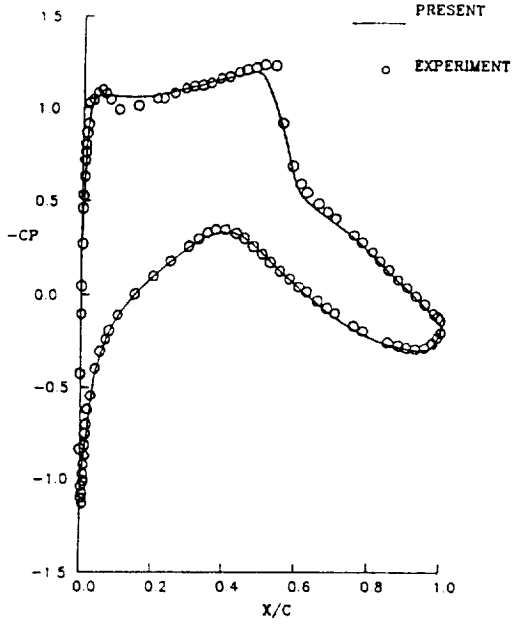

4. Surface Pressure Distribution over a RAE 2822 Airfoil at M_∞ = 0.725, α = 2.92 degrees, Re = 6.5 Million.

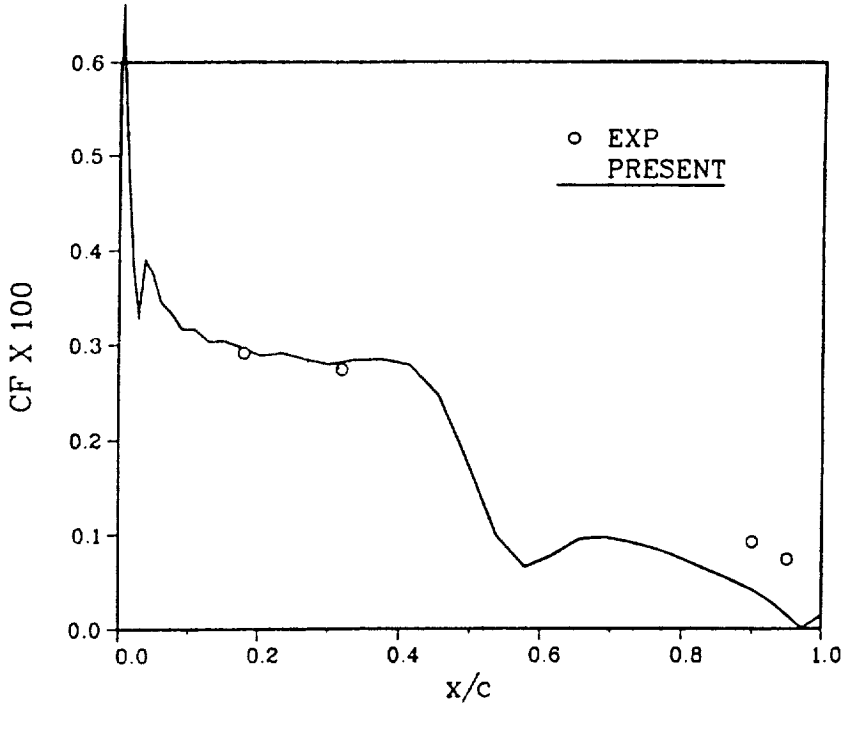

5. Velocity Profiles and Skin Friction Distribution for Conditions shown on Figure 4.

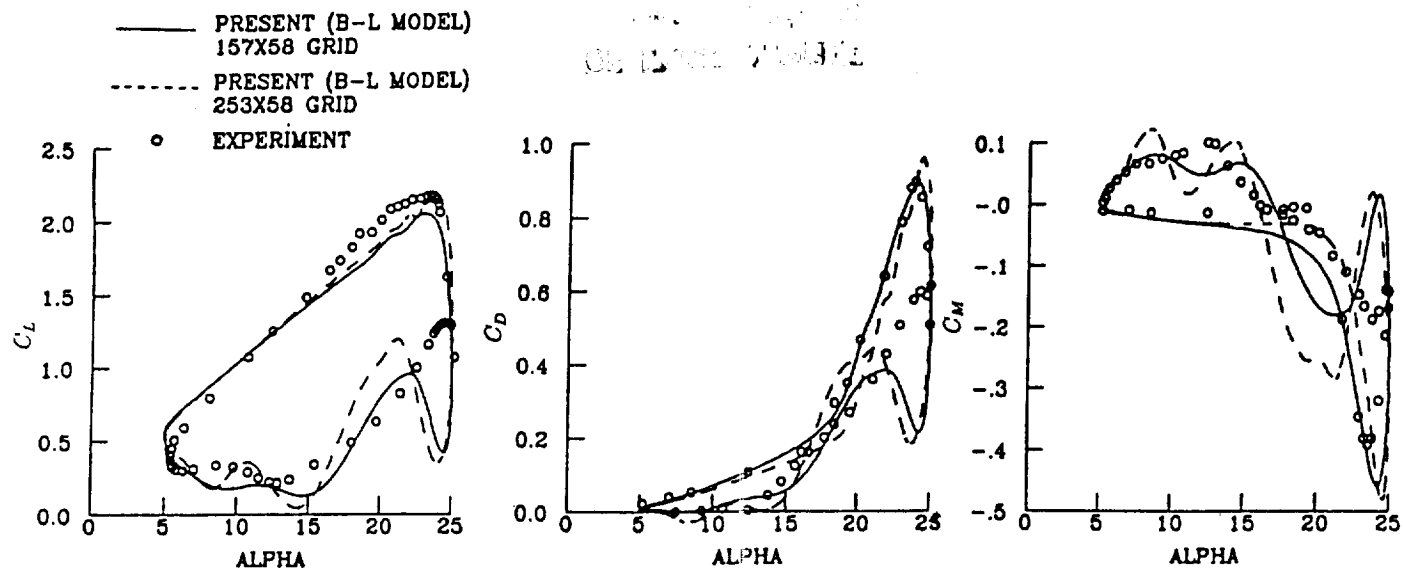

6. Computed and Measured Loads for a NACA 0012 Airfoil at Deep Dynamic Stall Condition. M_∞ = 0.283, Re = 3.45 Million , Reduced Frequency 0.151.

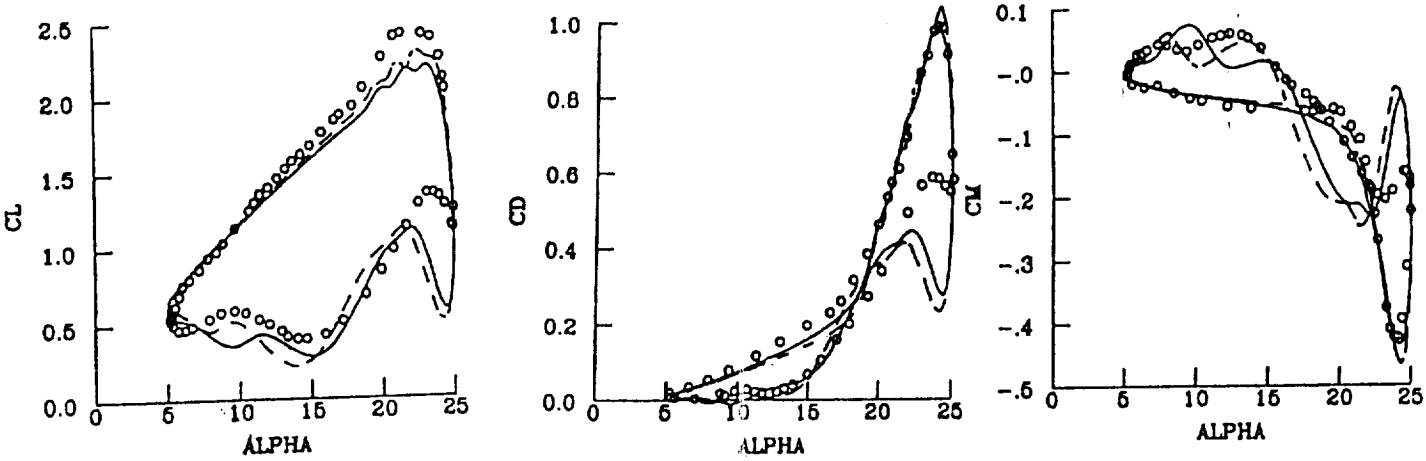

7. Computed and Measured Loads for a Hughes HH-02 Airfoil at Deep Dynamic Stall Condition. M_∞ = 0.283, Re = 3.45 Million , Reduced Frequency 0.151.

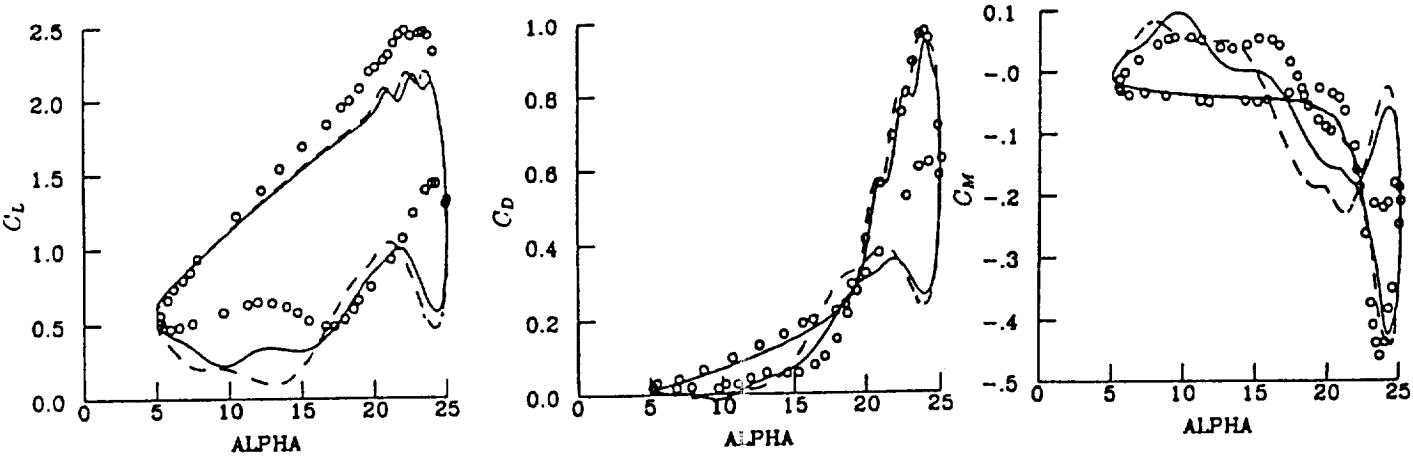

8. Computed and Measured Loads for a SC-1095 Airfoil at Deep Dynamic Stall Condition. M_∞ = 0.283, Re = 3.45 Million , Reduced Frequency 0.151.

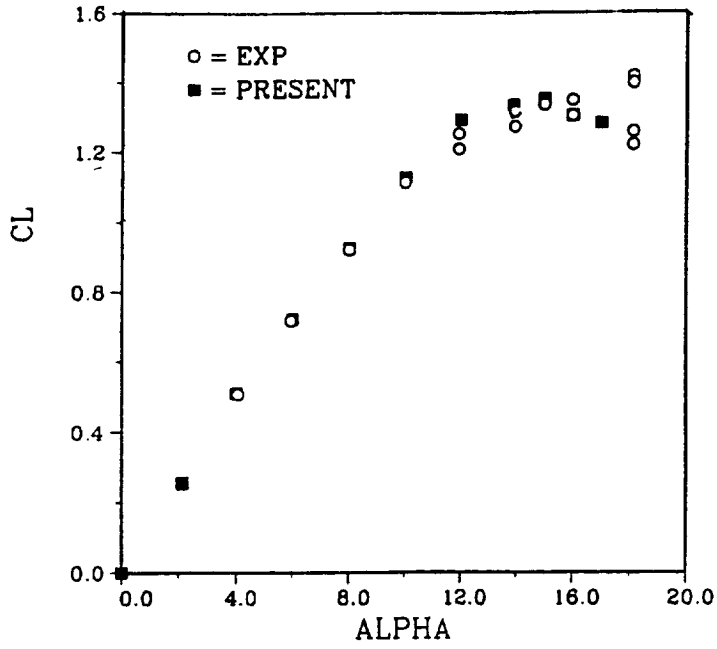

9. Lift vs. Angle of Attack over a NACA 0012 Airfoil at 30 degree yaw. Chordwise Mach Number 0.346, Re = 2.77 Million.

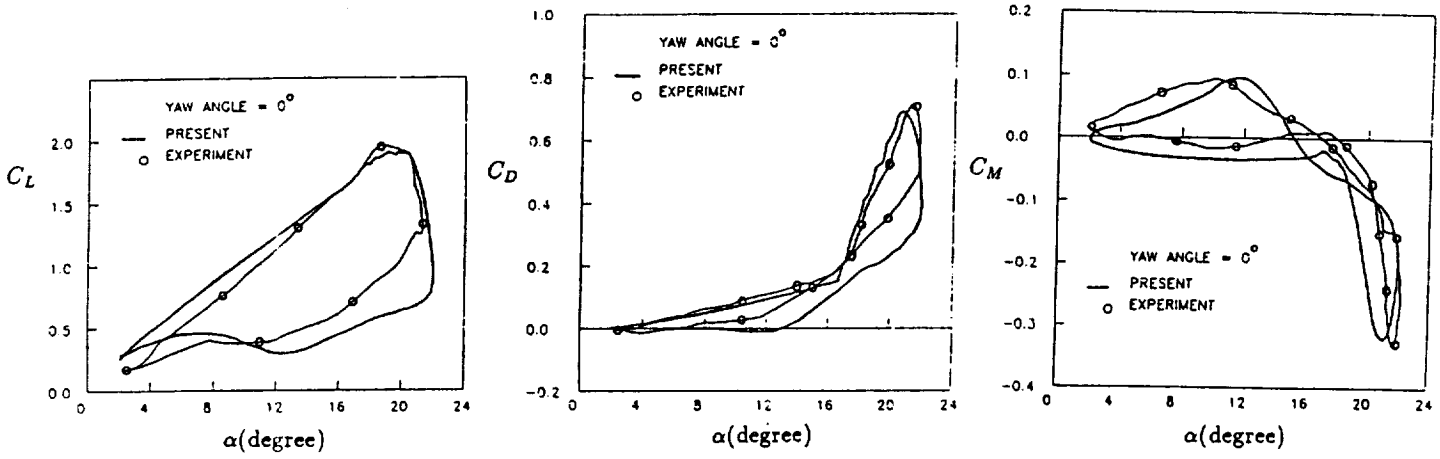

10. Computed and Measured Loads for a NACA 0012 Airfoil at Deep Dynamic Stall Condition. M_∞ = 0.3, Re = 2.77 Million , Reduced Frequency 0.124 , Zero Yaw.

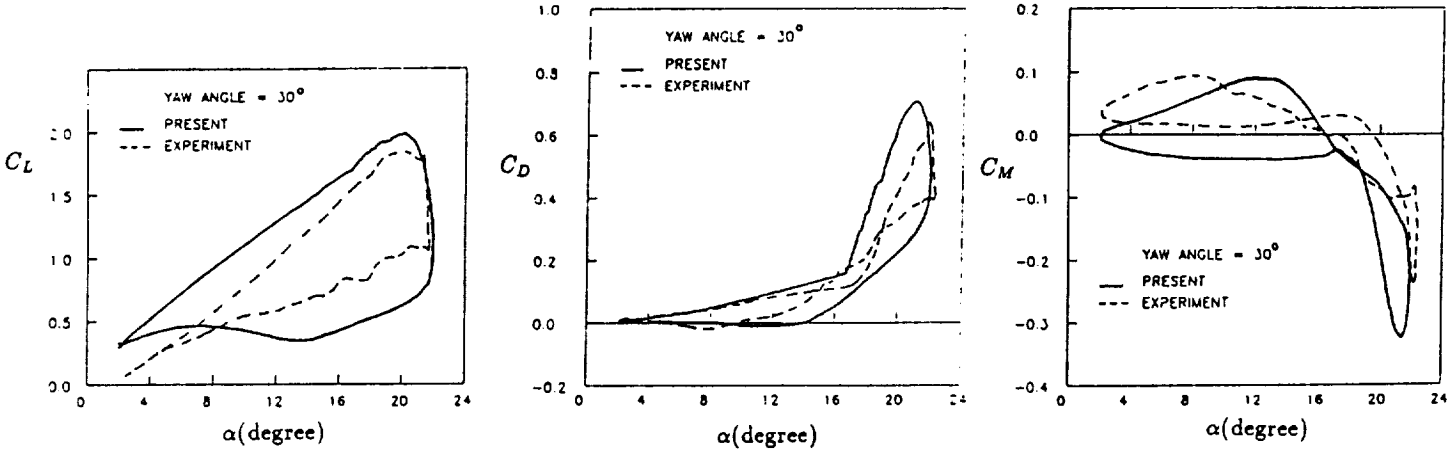

11. Computed and Measured Loads for a NACA 0012 Airfoil at Deep Dynamic Stall Condition. M_∞ = 0.3, Re = 2.77 Million , Reduced Frequency 0.124 , 30 degree Yaw.

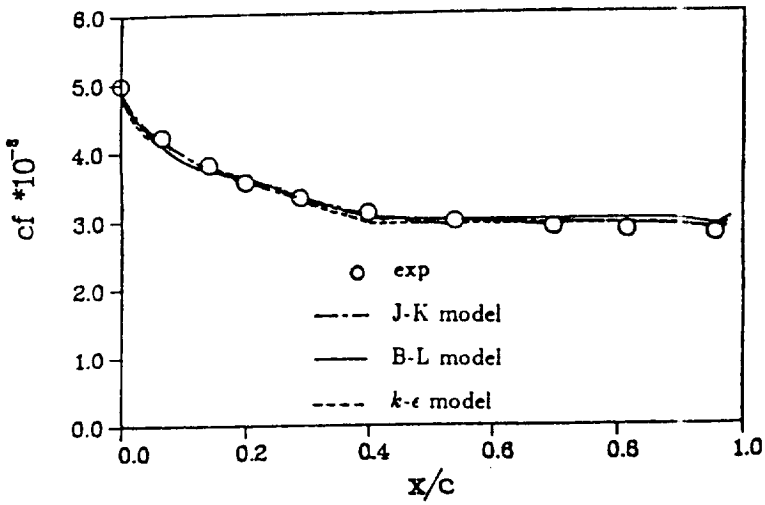

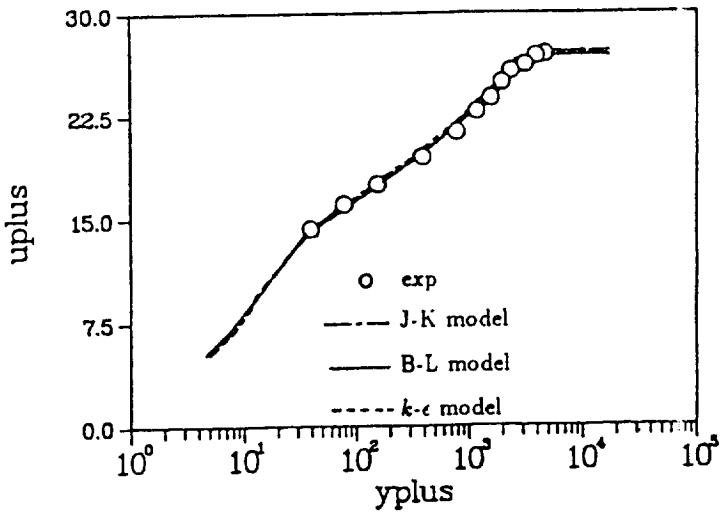

12. Surface Skin Friction and Velocity Profile Comparisons for a Flow over a Flat Plate. M_∞ = 0.1 , Re = 5 Million.

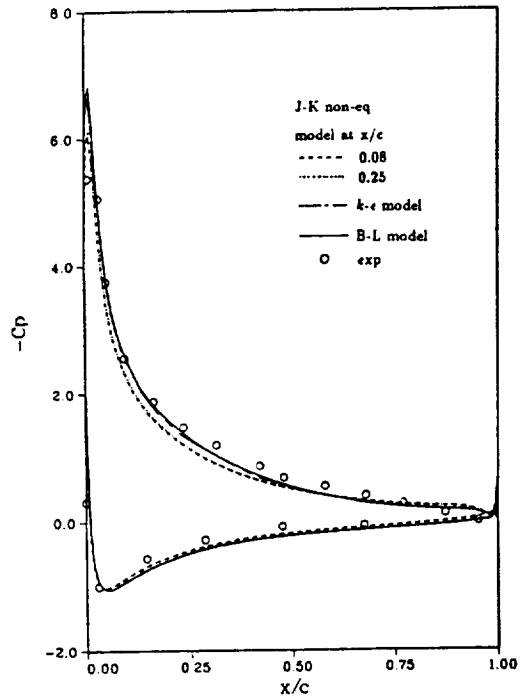

13. Flow over a NACA 0012 Airfoil at 13.5 degree angle of attack; 0.3 Mach Number; 3.9 Million Reynolds Number.

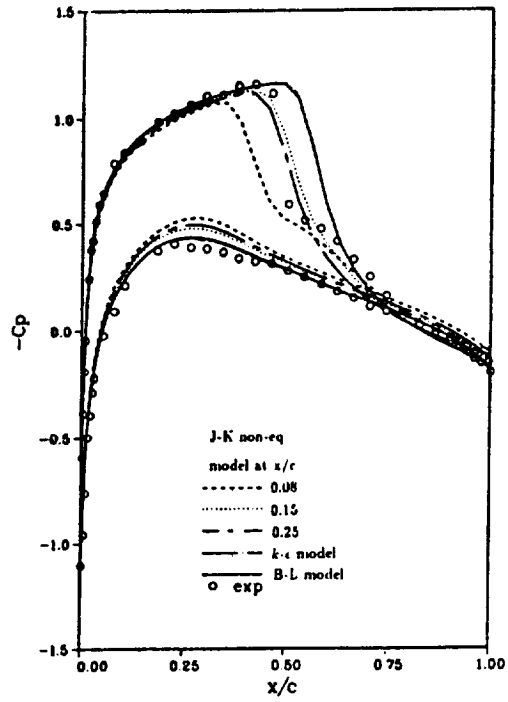

14. Flow over a NACA 0012 Airfoil at 2.66 degree angle of attack; 0.799 Mach Number; 9 Million Reynolds Number.

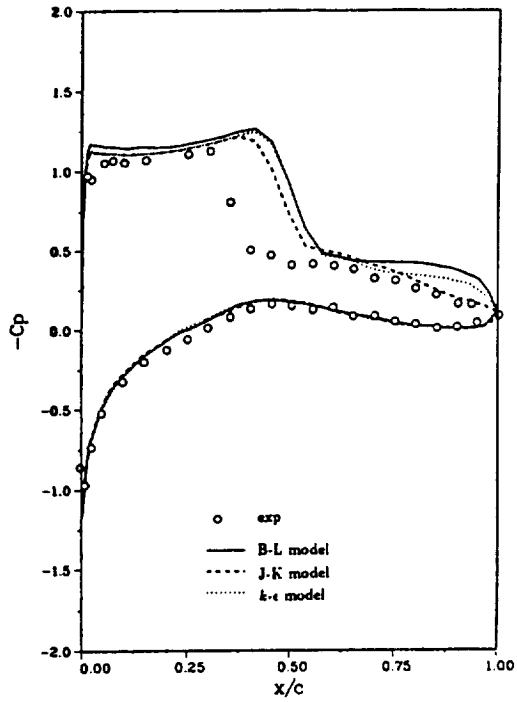

15. Flow over a NACA 64A010 Airfoil at 6.2 degree angle of attack; 0.8 Mach Number; 2 Million Reynolds Number.

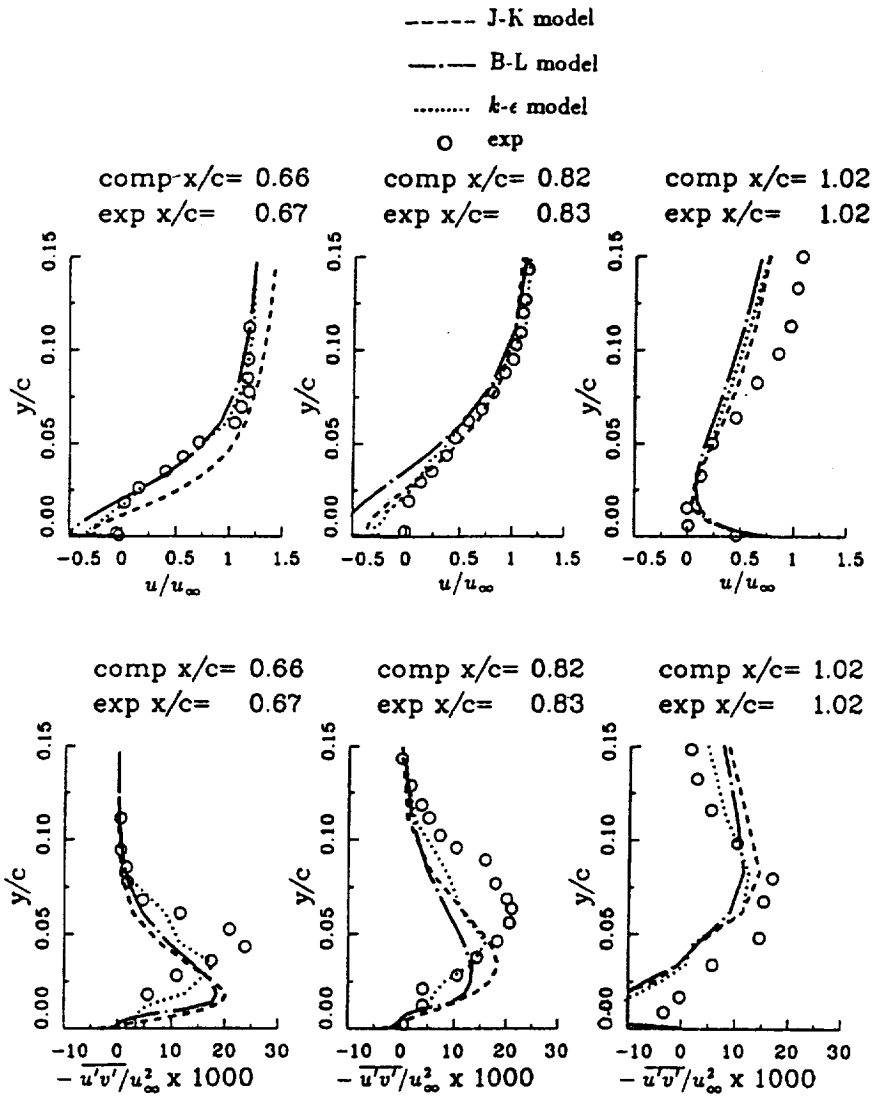

16. Velocity and Reynolds Stress Profiles for Conditions shown on Figure 15.

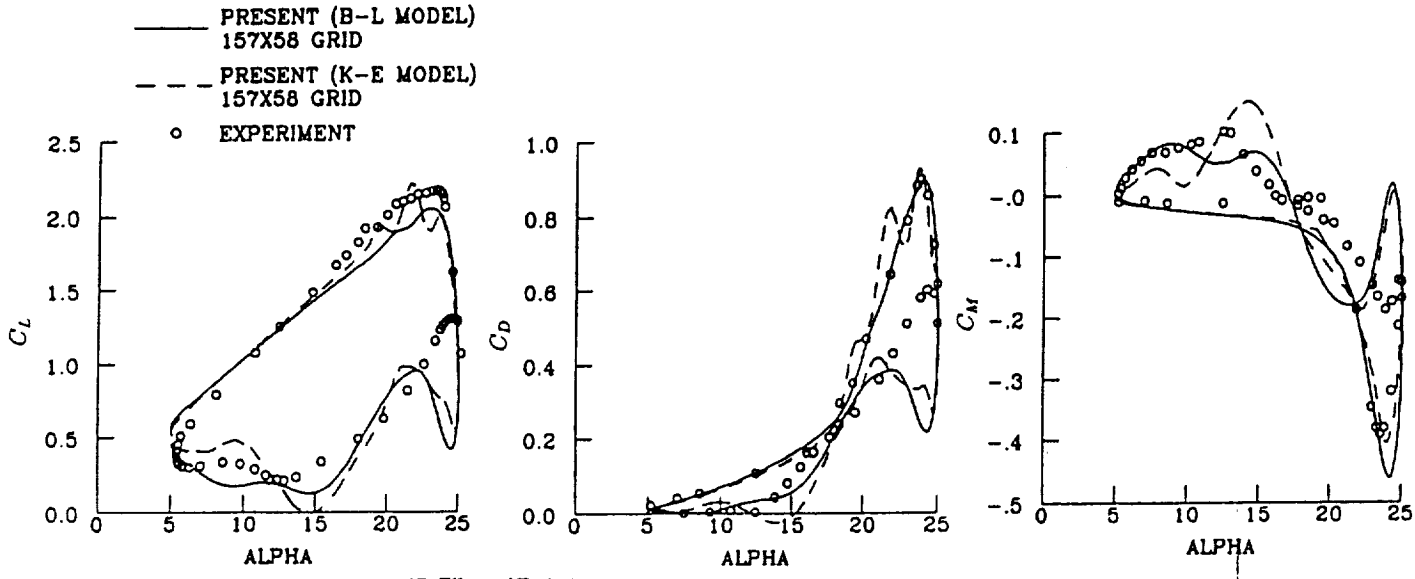

17. Effect of Turbulence Model on Dynamic Stall Predictions; Flow Conditions same as Figure 6.

NASA
National Aeronautics and Space Administration

Report Documentation Page

1. Report No.	2. Government Accession No.	3. Recipient's Catalog No.
NASA TM-101413 AIAA-89-0609		

4. Title and Subtitle

Evaluation of Three Turbulence Models for the Prediction of Steady and Unsteady Airloads

5. Report Date

6. Performing Organization Code

7. Author(s)

Jiunn-Chi Wu, Dennis L. Huff, and L.N. Sankar

8. Performing Organization Report No.

E-4507

10. Work Unit No.

505-90-01

9. Performing Organization Name and Address

National Aeronautics and Space Administration
Lewis Research Center
Cleveland, Ohio 44135-3191

11. Contract or Grant No.

13. Type of Report and Period Covered

Technical Memorandum

12. Sponsoring Agency Name and Address

National Aeronautics and Space Administration
Washington, D.C. 20546-0001

14. Sponsoring Agency Code

15. Supplementary Notes

Prepared for the 27th Aerospace Sciences Meeting sponsored by the American Institute of Aeronautics and Astronautics, Reno, Nevada, January 9-12, 1989. Jiunn-Chi Wu and L.N. Sankar, Georgia Institute of Technology, School of Aerospace Engineering, Atlanta, Georgia 30332 (work funded under NASA Grant NAG3-768); Dennis L. Huff, NASA Lewis Research Center

16. Abstract

Two-dimensional and quasi-3D Navier-Stokes solvers have been used to predict the static and dynamic airload characteristics of airfoils. The following three turbulence models were used: (1) Baldwin-Lomax algebraic model, (2) Johnson-King ODE model for maximum turbulent shear stress and (3) A two equation k-e model with law-of-the-wall boundary conditions. It was found that in attached flow the three models gave good agreement with experimental data. In unsteady separated flows, these models gave only a fair correlation with experimental data.

17. Key Words (Suggested by Author(s))	18 Distribution Statement
Navier-Stokes equations; Turbulence models; Dynamic stall; Airfoils	Unclassified – Unlimited Subject Category 02

19. Security Classif. (of this report)	20. Security Classif. (of this page)	21. No of pages	22. Price*
Unclassified	Unclassified	12	A03

*For sale by the National Technical Information Service, Springfield, Virginia 22161